CERN Summer Student Programme 2017
Project Report

Characterisation of the VMM3 Front-end read-out ASIC

Student: Lara M. Bartels
E-Mail: lara.maria.bartels@gmx.net
Supervisor: Michael Lupberger

Contents

1 Introduction

This research project was conducted in the RD51 collaboration at CERN, which is involved in the development of micropattern gaseous detector technologies and read-out systems. One example in the broad range of possible applications of such gaseous detectors is the NMX macromolecular diffractometer instrument planned for the European spallation source (ESS) which is currently under construction in Lund, Sweden. For the NMX instrument neutron detectors with high rate capabilities, high stability and excellent spatial resolution are required. A group working in the RD51 collaboration at CERN within the BrightnESS project aims to fulfil those requirements using gas electron multiplier (GEM) detectors with Gadolinium foils as neutron converters [PFE]. In order to match the high rate capability of the detectors, new front-end read-out systems need to be tested and implemented. This project aims to understand and test the capabilities of the VMM3 as the front-end read-out ASIC for GEM detectors.

2 The VMM3 ASIC

The VMM3 is a front-end read-out ASIC developed for the New Small Wheel upgrade of the ATLAS experiment at the LHC. Its overall task is to filter and convert the analog output from the detector into streams of digital data. Figure 1 shows the architecture of the VMM3. The aspects of the VMM3 which are not relevant for this project are only shown faded out for completeness. The features seen within the red box are repeated for each of the 64 channels per hybrid. Going from left to right, the incoming analog signal from the corresponding detector anode strip is first amplified by a charge amplifier and then shaped and changed in width by a shaper. The width can be adjusted by choosing different peaking times. A discriminator compares the height of the signal to a given threshold. If the threshold is crossed, the peak amplitude and time are recorded using a peak and time detector. The threshold can be adjusted individually for each of the channels using the trimmer. The discriminator is also connected to a neighbouring logic. If neighbouring is enabled and a hit is recorded in one of the channels, the read-out of the two adjacent channels is forced as well, even if their threshold was not crossed. The peak detector saves the peak amplitude of the signal to analog memory, which is converted to a digital signal by a 10 bit analog to digital converter (ADC). The data read-out for each of the 64 channels is also shown in Figure 2. The measurement of the time consists of two different values. The BCID is given by a counter which is increased at each tick of the CKBC clock. For the CKBC clock frequency values of 10, 20 or 40 MHz are usually chosen. The resolution of the counter is 12 bit resulting in BCID values between 0 and 4095. The read-out frequency has to be adapted to the CKBC frequency in order to avoid overflow of the BCID values. The time resolution given by the BCID depends on the CKBC clock frequency. The CKBC values given above correspond to a period of 100, 50 or 25 ns between two BCIDs. In order to achieve even higher precision in the time measurement, a time to amplitude converter (TAC) is used. As seen in Figure 2 the TAC starts ramping up a voltage at a given time which can be chosen either to be the time at which the signal crosses the threshold or reaches its peak amplitude. The ramp stops as soon as either its maximum value is reached or at the falling edge of the next CKBC signal. The ramp duration which will be referred to as TAC slope from here on, can be chosen from a given list of values (60, 100, 350 and 650 ns). The voltage level at the end of the ramp is digitalised using an 8 bit ADC, resulting in TDC values between 0 and 255. The data is sent out in two simultaneous data streams to enable higher rates. The first bit of the DATA0 stream is an event flag that announced the incoming datastream. The second datastream begins with the over threshold bit, which indicates whether the event crossed the threshold (1) or the read-out was forced through the neighbouring logic (0). The stream also contains the channel, time and amplitude information for the event corresponding to a total of 38 bits.

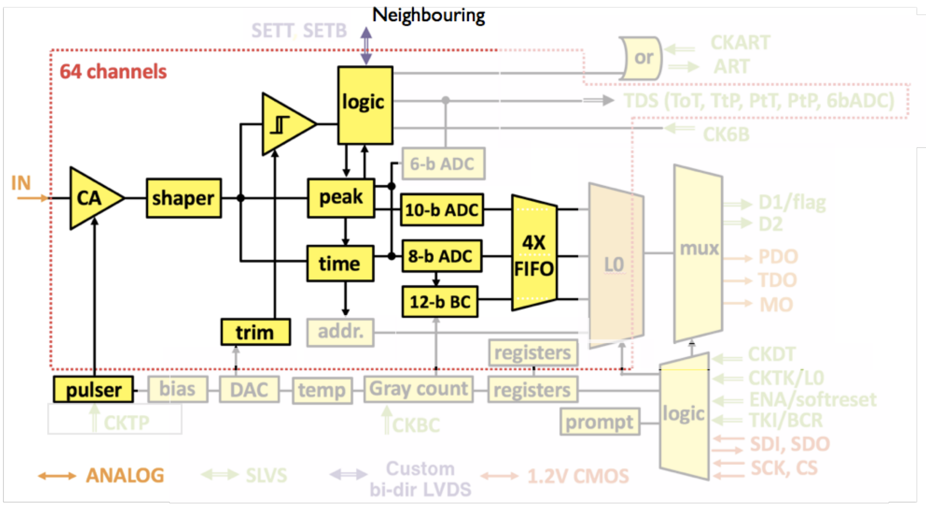

Figure 1: Overview of the VMM3 architecture [VMM].

For testing and calibration purposes, the VMM3 also contains a pulser which sends test pulses to the channels at given intervals. For data acquisition the VMM3 provides two different modes, a continuous and an external trigger based mode. While in the continuous mode, data is read out in a given interval of time, in the external trigger mode, read-out occurs only after a signal from an external trigger detector [VMM]. The datastream from the VMM3 hybrid is sent out to the next step of the read-out chain, the scalable read-out system (SRS). The SRS perform further processing, adds an additional SRS timestamp for each read-out period and sends the data to a computer in UDP packages. The data from the UDP packages is then written into .csv files, the format of which can be seen in Figure 3. From left to right, the csv file contains the FEC number, the VMM number, channel, SRS Timestamp, BCID, TDC, ADC and over threshold flag for each event.

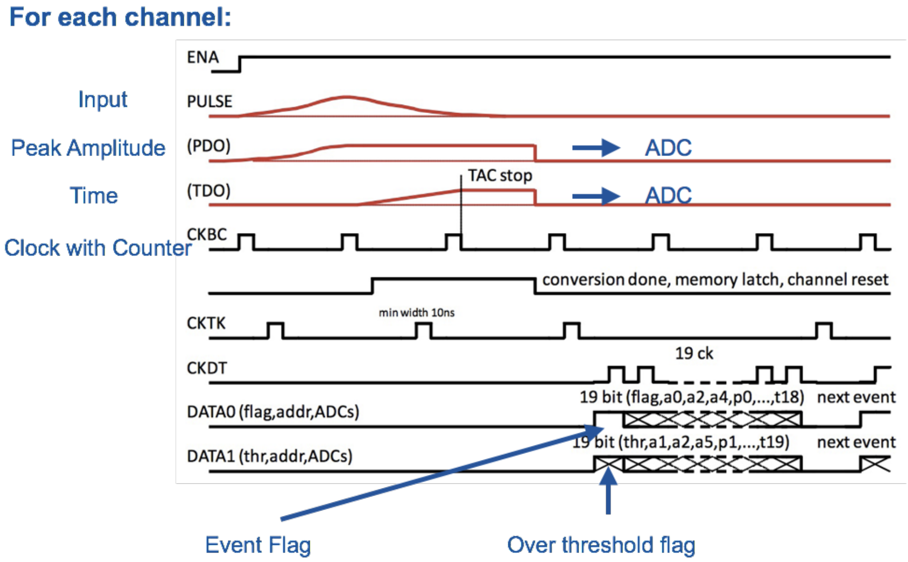

Figure 2: Overview of data read-out of the different components of the VMM3 [VMM].

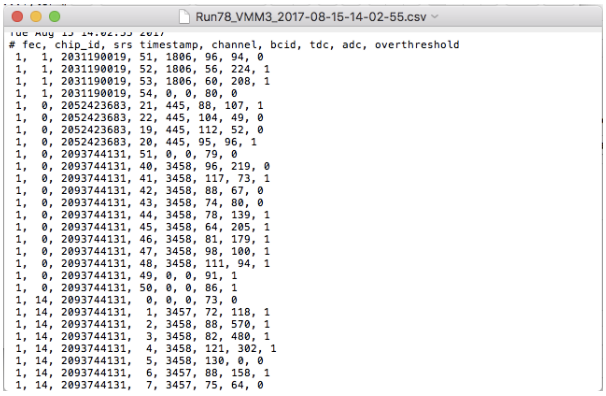

Run78_VMM3_2017-08-15-14-02-55.csv

```
# fec, chip_id, srs timestamp, channel, bcid, tdc, adc, overthreshold
 1,  1, 2031190019, 51, 1806, 96, 94, 0
 1,  1, 2031190019, 52, 1806, 56, 224, 1
 1,  1, 2031190019, 53, 1806, 60, 208, 1
 1,  1, 2031190019, 54, 0, 0, 80, 0
 1,  0, 2052423683, 21, 445, 88, 107, 1
 1,  0, 2052423683, 22, 445, 104, 49, 0
 1,  0, 2052423683, 19, 445, 112, 52, 0
 1,  0, 2052423683, 20, 445, 95, 96, 1
 1,  0, 2093744131, 51, 0, 0, 79, 0
 1,  0, 2093744131, 40, 3458, 96, 219, 0
 1,  0, 2093744131, 41, 3458, 117, 73, 1
 1,  0, 2093744131, 42, 3458, 88, 67, 0
 1,  0, 2093744131, 43, 3458, 74, 80, 0
 1,  0, 2093744131, 44, 3458, 78, 139, 1
 1,  0, 2093744131, 45, 3458, 64, 205, 1
 1,  0, 2093744131, 46, 3458, 81, 179, 1
 1,  0, 2093744131, 47, 3458, 98, 100, 1
 1,  0, 2093744131, 48, 3458, 111, 94, 1
 1,  0, 2093744131, 49, 0, 0, 91, 1
 1,  0, 2093744131, 50, 0, 0, 86, 1
 1, 14, 2093744131,  0, 0, 0, 73, 0
 1, 14, 2093744131,  1, 3457, 72, 118, 1
 1, 14, 2093744131,  2, 3458, 88, 570, 1
 1, 14, 2093744131,  3, 3458, 82, 480, 1
 1, 14, 2093744131,  4, 3458, 121, 302, 1
 1, 14, 2093744131,  5, 3458, 130, 0, 0
 1, 14, 2093744131,  6, 3457, 88, 158, 1
 1, 14, 2093744131,  7, 3457, 75, 64, 0
```

Figure 3: Example of the beginning of a .csv file recorded during the test beam in August.

The incoming UDP packages are monitored using a designated wireshark plugin. This shows the number of hits as well as all the information associated with them. The wireshark tool is mainly used for short tests of the using test pulses in the lab or during setup at the test beam.

3 Test Beam Set-up

The performance of the VMM3 was tested during two test beam times in July and August. The set-up for the July test-beam is shown in figure 4.

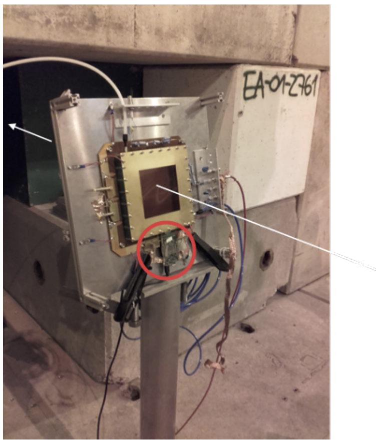

Figure 4: Set-up for the test beam in July in the North Area. One VMM3 hybrid (red circle) is connected to a standard triple GEM exposed to a muon beam (white arrow).

Data was recorded using one VMM3 hybrid in a muon test beam with a standard triple GEM. Therefore only one-dimensional read-out was possible during the July test beam. The runs recorded in July were mainly a proof of principle for different settings of the VMM3 and had the goal to successfully demonstrate first data acquisition using the hybrid as the front-end read-out for GEMs. The longer test beam in August allowed for a more rigorous and structured testing of different settings of the VMM. In addition, data was recorded in a pion beam enabling tests of the high rate capabilities of the VMM3. During the first runs two VMM3 hybrids were used, enabling read-out in two dimesions X and Y (5a). For the last runs a third hybrid was added in X dimension (5b) resulting in 256 read-out channels in the X-dimension and 128 in Y. The muon and pion test beams in the North area are not continuous, but consist of spills originating from a fixed target and occurring in intervals of fractions of minutes. The spill frequency may also vary during operation, depending on the performance of the accelerators and instruments.

4 Results and Discussion

While the goal for the test beam in July was mainly to demonstrate the capability of slow control and data acquisition with the VMM3 as the front-end read-out of a GEM detector in a test beam setting, the longer test beam in August enabled longer and more systematic studies of the different settings of the VMM3. Therefore in this section only the results from the August test beam data will be presented.

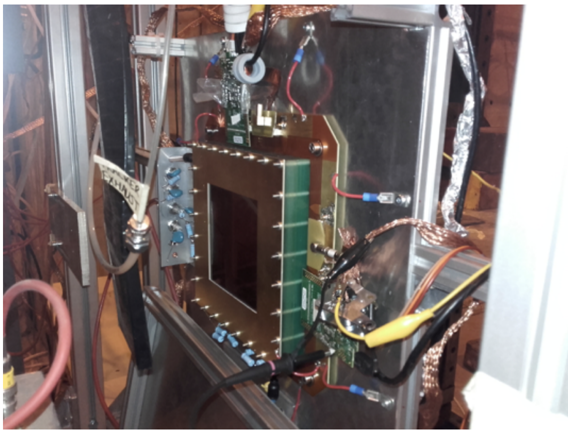

(a) Two hybrids

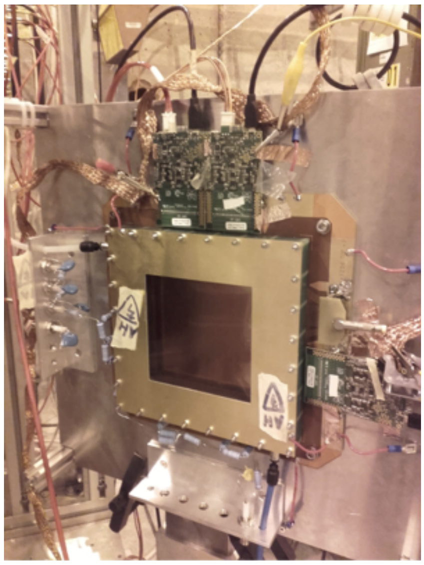

(b) Three hybrids

Figure 5: Set-up for the test beam in August in the North Area. Data was recorded with a standard triple GEM exposed to a muon or pion beam and read out with two (a) or three (b) VMM3 hybrids.

4.1 Analysis Output

In this section an overview of the output generated in the analysis is shown for one of the runs. Run number 80 was chosen, as a muon beam in combination with the most standard settings (CKBC= 20 MHz. TAC Slope= 60 ns, Peaking Time= 100 ns) were used and data was taken over a relatively long period of time. For each VMM3 hybrid histograms of the ADC, TDC, BCID, SRS timestamps, and channels are produced. These are shown in Figures 6. In addition, the average of the ADC, TDC and BCID values is calculated for each channel and plotted as shown in Figure 7. For the SRS timestamps a histogram of the SRS timestamp histogram is created in order to obtain the distribution of the number of hits per SRS timestamp, as shown in Figure 8a. All histograms are created using the pyROOT and root numpy packages and are saved in a pdf as well as a ROOT format to enable a more detailed inspection later on. From the data contained in the TDC spectra for each channel the minimum and maximum TDC value is extracted. TDC values that occur less often than a given finite number of minimum occurrences are discarded for this range determination. The minimum and maximum values are then plotted over the channels as seen in 8b.

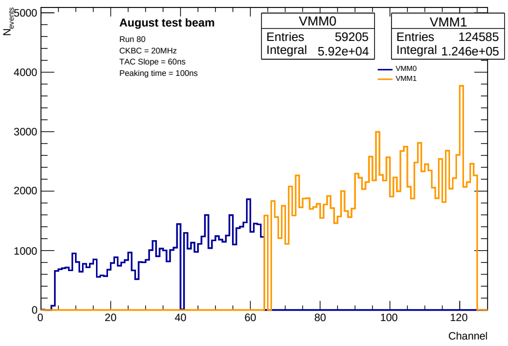

(a) Channels

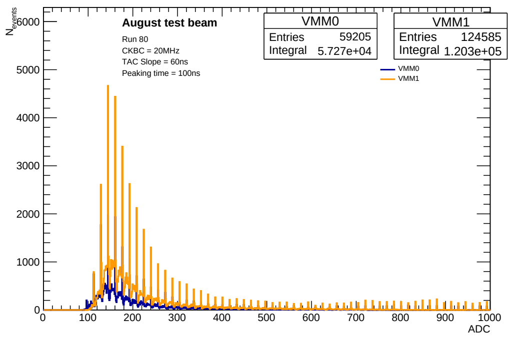

(b) ADC

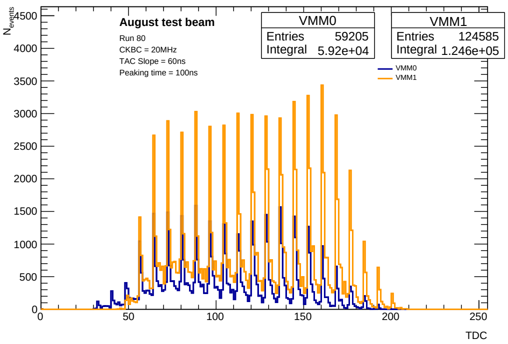

(c) TDC

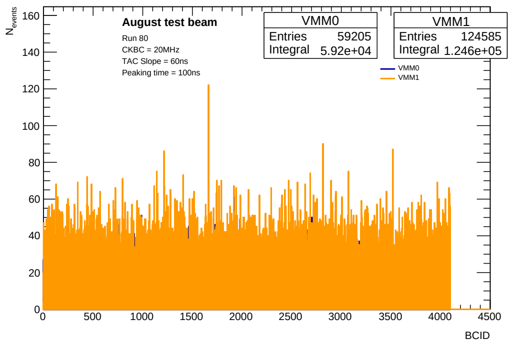

(d) BCID

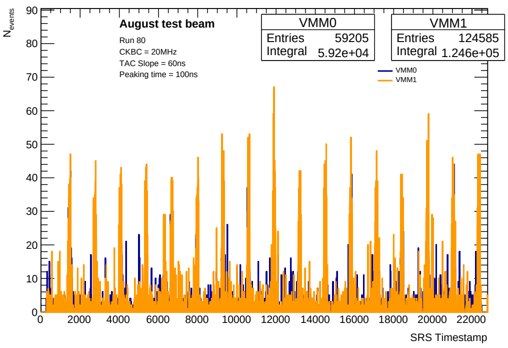

(e) SRS timestamp

Figure 6: Output histograms from the analysis of test beam run 80. Histograms of the Channels (a), ADC (b), TDC (c), BCID (d) and SRS timestamps (e) are created.

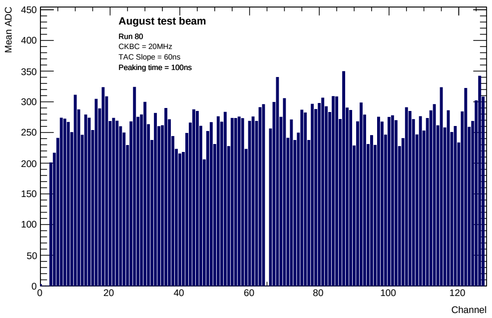

(a) ADC

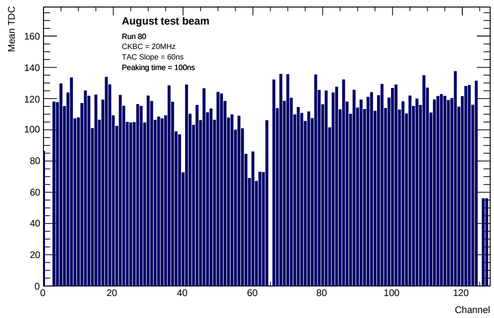

(b) TDC

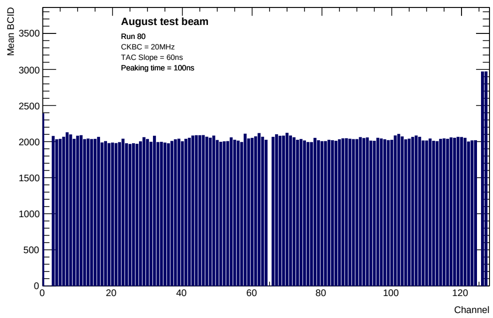

(c) BCID

Figure 7: Output histograms from the analysis of test beam run 80. Histograms of the Channels (a), ADC (b), TDC (c), BCID (d) and SRS timestamps (e) are created.

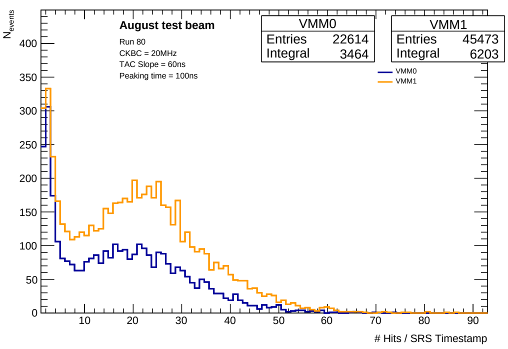

(a) SRS Hits

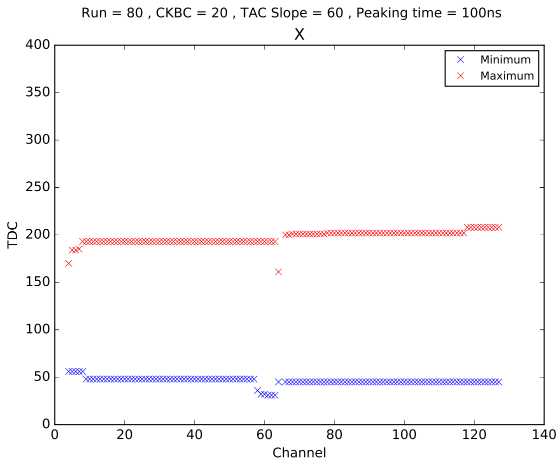

(b) TDC

Figure 8: The plot (a) shows a histogram of the number of Hits recorded per SRS timestamp. Plot (b) shows the minimum and maximum TDC value recorded plotted over the channels.

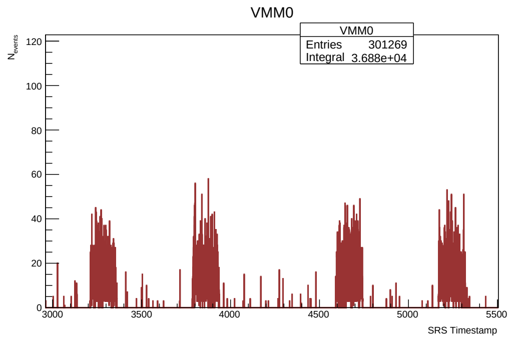

(a) Muon spills

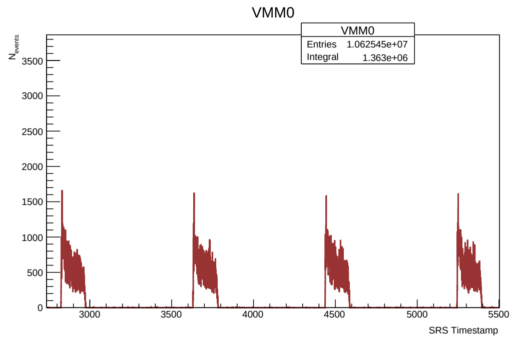

(b) Pion spills

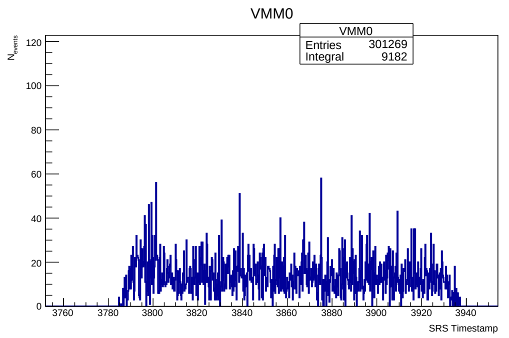

(c) Muon spill close up

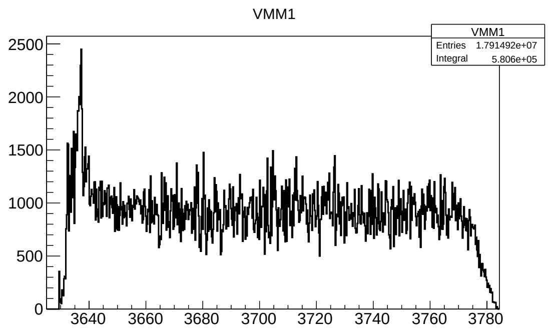

(d) Pion spill close up

Figure 9: The number of Hits is plotted over the SRS timestamps. While Figures (a) and (c) depict muon spills, Figures (b) and (d) stem from data recorded in a pion beam. Figures (a) and (b) give an overview over the spill structure of the beam and the ratio of time and without spills occurring. The width of the x-axis corresponds to a time period of roughly 80 s. Figures (c) and (d) each show a close up plot of an individual spill.

4.2 Comparison of muon and pion beams

In Figures 9a and 9b the periodicity and shape of the muon and pion spills are clearly visible. The spill structure can be further compared in Figure 9c and 9d which shows a close up of a muon and a pion spill. There is a definite difference in the structure of the individual spills. For the pion beam there is a distinctive peak at the beginning of each spill followed by a gradual decrease over the duration of the spill. The muon spills show a much more diverse structure that may differ from spill to spill. The key difference between the measurements in muon and pion beams using the VMM3 are the hit rates. Figures 10a and 10b show the hits per SRS timestamp for data recorded in muon and pion beams. The peak value is translated into a hit frequency which is in turn converted into the corresponding bit-rate assuming 38 bits per event. The rates calculated for the pion beams are larger by one order of magnitude.

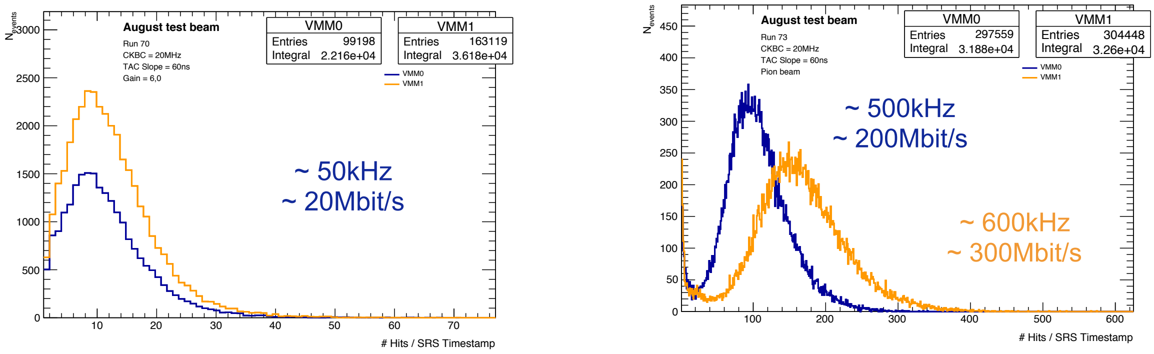

(a) Muons **(b)** Pions

Figure 10: Histogram of the number of hits recorded per SRS timestamp for muons (a) and pions (b). The inset numbers show the hit and bit rates corresponding to the peak values.

4.3 Testing of miscellaneous settings

Figures 11a and 11c show the number of hits recorded plotted over the channels in X and Y direction. The overall shape of the distribution reflects the beam profile and thus the positioning of the detector with respect to the beam. The fluctuations between the channels are most likely due to differences in the baselines between the channels. A trimming of the thresholds can be performed for each channel individually. Following this equalising of thresholds, one would expect the distribution to smoothen out until the fluctuations between the channels are mostly of statistical nature or due to effects related to the detector itself.
Figure 11 demonstrates the effect of the neighbouring function on the distribution of hits over channels. In both runs data was taken using the same settings and over the same time period. The neighbouring function was disabled for the run shown in Figures 11a and 11c and enabled for the run shown in Figures 11b and 11d . Channels that appear to be dead when the neighbouring function is disabled and therefore never record hits which cross the threshold fit very well into the overall hit distribution when the neighbouring function is enabled. This provides further evidence for the threshold being set too high in some of the channels. Therefore the apparent positive effect of enabling the neighbouring logic might be significantly reduced once channel trimming is performed and all threshold are equalised. As a perfect trimming of the thresholds is impossible to perform and one cannot exclude other factors contributing to the observed effect, a new comparison of data recorded with and without enabling the neighbouring logic after the channel trimming is necessary. The forced read-out of neighbouring channels might then still turn out be beneficent to the data taking process by reducing the loss of valuable data or detrimental by adding noise.

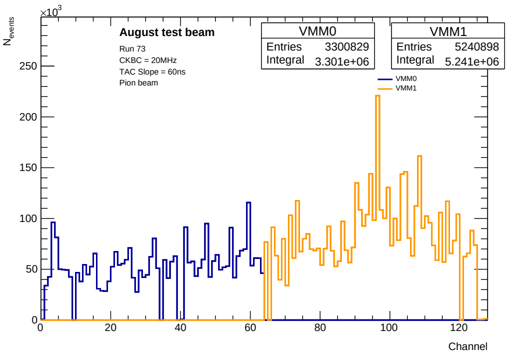

(a) X dimension, Neighbouring logic disabled.

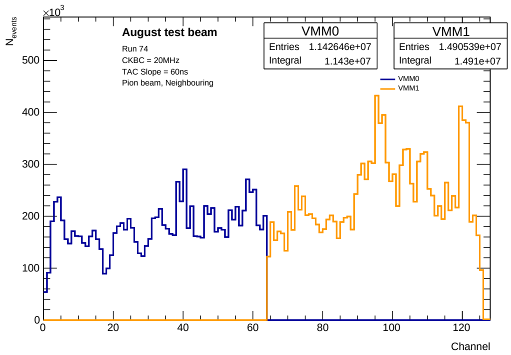

(b) X dimension, Neighbouring logic enabled.

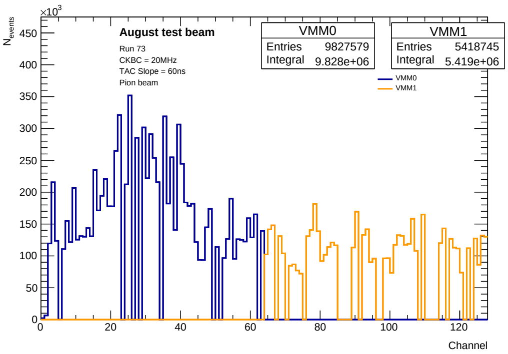

(c) Y dimension, Neighbouring logic disabled.

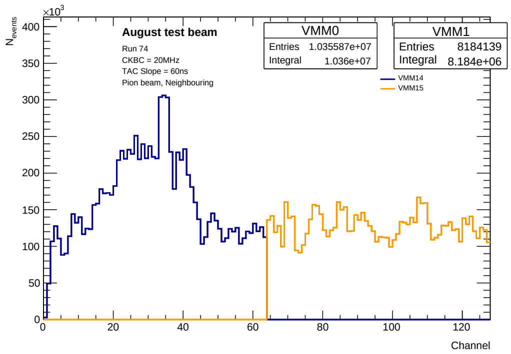

(d) Y dimension, Neighbouring logic enabled.

Figure 11: Histograms showing the total number of hits recorded in a pion beam for each channel in X (a and b) as well as in Y (c and d) direction. For Figures (a) and (c) the neighbouring logic was disabled, in Figures (b) and (d) the neighbouring logic was enabled. The remaining settings for the two runs were equal to the standard settings.

4.4 SRS Timestamp

The SRS Timestamp values overflow approximately every 13 seconds and the recorded data has to be corrected for this overflow. This is done by adding the maximum possible value of the SRS timestamps to all following values wherever a timestamp is lower than that of the preceding event. In Figure 9 the number of hits is plotted over the corrected SRS timestamp for data recorded in a muon and a pion beam. While the periodic spill structure of the beam is nicely portrayed in the muon run, the structure is lost in case of the pion beam data, if no additional corrections are applied to the data. This is due to the events written into the csv file not being perfectly sorted by their SRS timestamp at these high rates. This results in the occurrence of apparent overflows of the SRS timestamp resulting in an incorrect overflow correction and thus a displacement of chunks of data with respect to each other. Two additional conditions were implemented to ensure that an apparent overflow is not caused by shifted values, but is caused by the SRS timestamp having reached its maximum value. The first condition is a minimum difference of between the values just before and after the overflow. This excludes apparent overflows resulting from the swapping of two events. In addition to the swapping of individual events, entire chunks of data appear out of place as seen in Figure 12 with the SRS timestamp values just behind the chunk fit those just before. These chunks can be identified by comparing the SRS timestamp values before and after the SRS timestamp value following the overflow. When the overflow identification is corrected using these two conditions, the corresponding plot of the hits over the SRS timestamp reflects the spill structure again, confirming a successful correction.
The origin of the position shifting in the data is not the VMM3, but the process of writing the data into the csv files. The data recorded in the pion beam therefore successfully demonstrated the hight rate capabilities of the VMM3 up to the order of GHz for peak values.

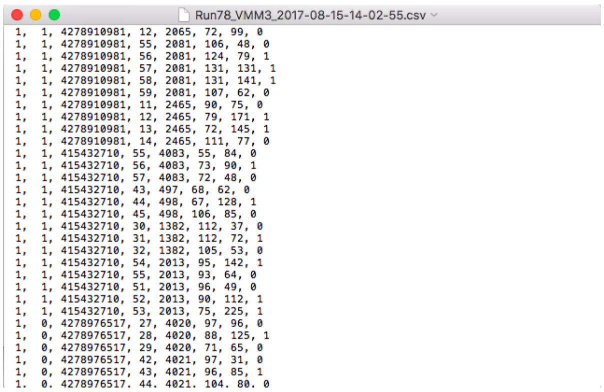
Run78_VMM3_2017-08-15-14-02-55.csv

```
1,  1, 4278910981, 12, 2065, 72, 99, 0
1,  1, 4278910981, 55, 2081, 106, 48, 0
1,  1, 4278910981, 56, 2081, 124, 79, 1
1,  1, 4278910981, 57, 2081, 131, 131, 1
1,  1, 4278910981, 58, 2081, 131, 141, 1
1,  1, 4278910981, 59, 2081, 107, 62, 0
1,  1, 4278910981, 11, 2465, 90, 75, 0
1,  1, 4278910981, 12, 2465, 79, 171, 1
1,  1, 4278910981, 13, 2465, 72, 145, 1
1,  1, 4278910981, 14, 2465, 111, 77, 0
1,  1, 415432710, 55, 4083, 55, 84, 0
1,  1, 415432710, 56, 4083, 73, 90, 1
1,  1, 415432710, 57, 4083, 72, 48, 0
1,  1, 415432710, 43, 497, 68, 62, 0
1,  1, 415432710, 44, 498, 67, 128, 1
1,  1, 415432710, 45, 498, 106, 85, 0
1,  1, 415432710, 30, 1382, 112, 37, 0
1,  1, 415432710, 31, 1382, 112, 72, 1
1,  1, 415432710, 32, 1382, 105, 53, 0
1,  1, 415432710, 54, 2013, 95, 142, 1
1,  1, 415432710, 55, 2013, 93, 64, 0
1,  1, 415432710, 51, 2013, 96, 49, 0
1,  1, 415432710, 52, 2013, 90, 112, 1
1,  1, 415432710, 53, 2013, 75, 225, 1
1,  0, 4278976517, 27, 4020, 97, 96, 0
1,  0, 4278976517, 28, 4020, 88, 125, 1
1,  0, 4278976517, 29, 4020, 71, 65, 0
1,  0, 4278976517, 42, 4021, 97, 31, 0
1,  0, 4278976517, 43, 4021, 96, 85, 1
1.  0. 4278976517. 44. 4021. 104. 80. 0
```

Figure 12: Small excerpt from one of the data files containing events recorded in a pion beam. One occurrence of an out of place chunk of data in the data file is shown.

4.5 Bit reduction

While the histogram of the hits over the SRS timestamp is expected to reflect the spill structure of the muon and pion beams, one would expect an even, uniform distribution of values for the more precise measurements within the allowed range of values of the BCID and TDC as the range of possible values is small compared to the duration of the spills. As seen in Figure 13, the spectra of the BCID, TDC and ADC show spikes at regular intervals. In these spikes the data missing from the surrounding bins appears to accumulate, resulting in some values being underrepresented and a consequent loss of precision in case of the ADC and TDC. The ADC spikes are found at multiples of 16, rendering the lower 4 bits of the 10 bit ADC value meaningless. For the TDC, the spikes occur at multiples of 8 rendering the lower 3 bits meaningless. Given the shortest ADC slope length of 60 ns this results in a reduction of the best possible time resolution of 0.25 ns to a resolution of about 2 ns. The spikes of the BCID spectra occur at less regular intervals. In the inset on the right of Figure 13c three of those spikes can be seen close up. As opposed to the spikes in the TDC and ADC spectra, the spikes in the BCID do not appear to accumulate data that is missing from a range of different values, but rather contain only the additional data form the following, empty bin. Therefore the consequences of those spikes are less severe for the BCID, as there is only a very limited number of bins affected while the spikes in the ADC and TDC are the result of a more global problem. Further issues observed in the BCID and TDC spectra are discussed in the following sections.

4.6 BCID

There are two more features of the BCID spectra to be described in addition to the spikes followed by empty bins mentioned in the previous subsection. First it is interesting to note that some spikes in the BCID spectrum are not followed by an empty bin. As these occur at BCIDs following the pattern of the other spikes, they are likely due to a related issue. Secondly, at BCID values of between $3100 - 3500$ an unexpected dip in values occurs, which can be seen clearly in the inset of Figure 14. The dip changes position slightly based on the read-out frequency, indicating a causal link between the two and calling for a more rigorous study of the correlation between the two.

4.7 TDC

As in the case of the BCID values, one would expect a uniform distributions of TDC values in the allowed range. However, while the range of the BCID values always stretches from 0 to 4095, the range of possible TDC values depends on the settings for TAC slope and CKBC. The inverse of the CKBC frequency gives the time between two clock ticks and as the TAC ramp stops at the next clock tick, it also corresponds to the maximum time that can be obtained using the TAC. For the standard CKBC frequency of 20 MHz

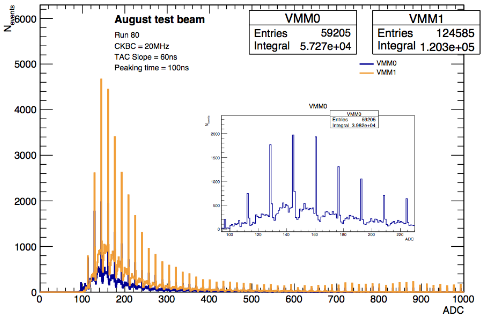

(a) ADC spectrum

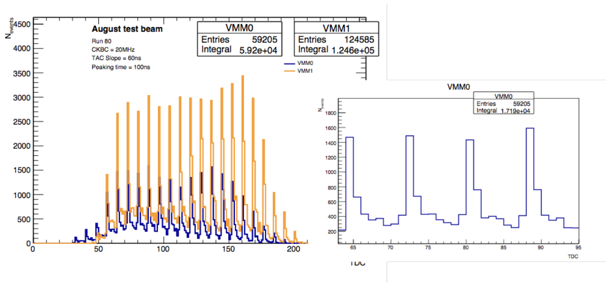

(b) TDC spectrum

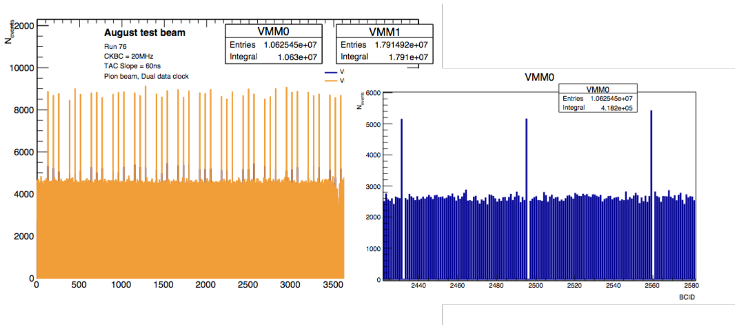

(c) BCID spectrum

Figure 13: Spectra of the ADC (a), TDC (b) and BCID (c) values with insets showing a close up of a selected range of values.

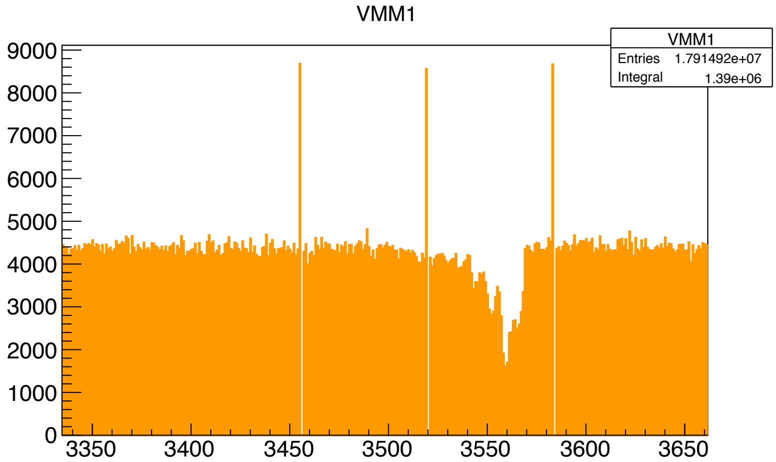

Figure 14: Zoom into the BCID spectrum plot showing an unexpected dip in values.

used in most of the measurements, even the shortest TAC slope of 60 ns is shorter than the time interval of 50 ns between two clock ticks. Therefore one would expect the TDC values to be uniformly distributed in an interval that stretches over $\frac{5}{6}$ of the total 256 values. This can indeed be seen in Figure 15. The TDC spectra become even more narrow for the larger TAC slope values, resulting in lower average TDC values for those settings. The average TDC values are plotted over the length of the TAC slope in Figure 16 show a linear correlation in good agreement with the expectations. The value range covered by the TDC values appears do differ between the VMMs. One of the possible causes of the shift between the spectra of different VMMs is a pedestal of the TDC, i.e. the TAC slope does not ramp up from 0, but rather a fixed finite voltage. These offsets may vary between the hybrids and even between the individual channels of one VMM, leading to the shift observed in the data. The offset does not however, pose an explanation for the differences in width of the spectra. In Figure 17b is one example for the TDC spectra recorded with the third hybrid. For the data obtained with VMM 7, the spectra have a distinctive peak at lower values in contrast to the approximately even distribution of the values for all other VMMs. As this problem only occurs for this specific VMM, it is probably not a general issue. The splitting of the value range into two subranges, one of them at very high values close to the maximum of 256, as seen in Figure 17c is observed for all of the VMMs. As it only occurs for a subset of runs, a comparison of the settings could yield a possible cause for the splitting.
Despite this good agreement some features of the TDC spectra have yet to be explained. Figure 17 show the TDC spectra for two VMMs. In Figure 17a a shift of the spectrum between the two VMMs can be clearly seen. In addition, the width of the interval covered by the TDC values appears do differ for the VMMs. One of the possible causes of the shift between the spectra of different VMMs is a pedestal of the TDC, i.e. the TAC slope does not ramp up from 0, but rather a fixed finite voltage. These offsets may vary

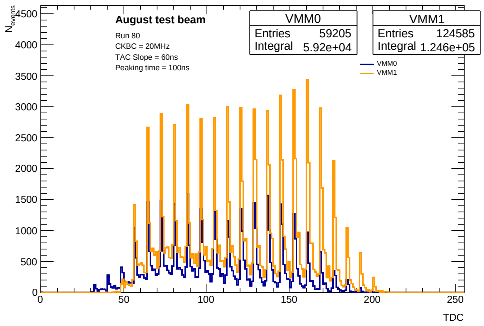

(a) TAC slope = 60 ns..

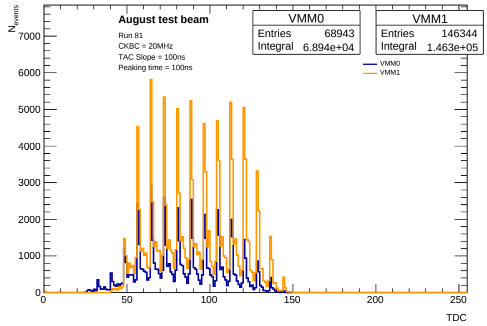

(b) TAC slope = 100 ns..

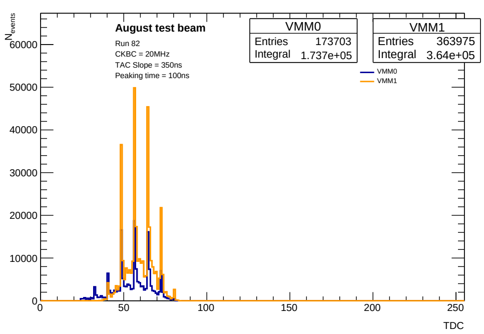

(c) TAC slope = 350 ns..

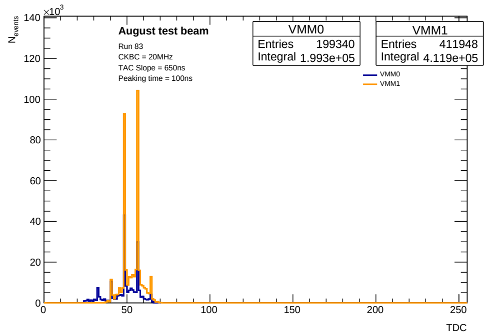

(d) TAC slope = 650 ns..

Figure 15: TDC spectra for two VMMs for the four different TAC slope values.

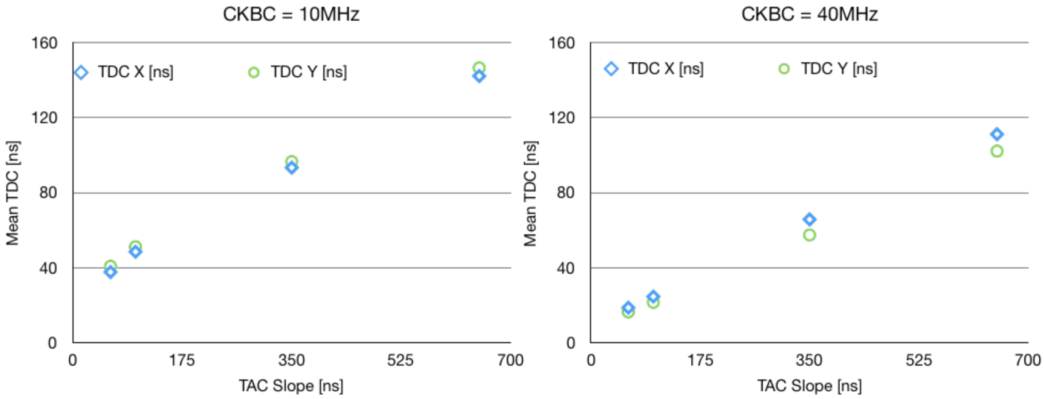

Figure 16: Average TDC values as a function of TAC slope length for two different CKBC frequencies.

between the hybrids and even between the individual channels of one VMM, leading to the shift observed in the data. The offset does not however, pose an explanation for the differences in width of the spectra. In Figure 17b is one example for the TDC spectra recorded with the third hybrid. For the data obtained with VMM 7, the spectra have a distinctive peak at lower values in contrast to the approximately even distribution of the values for all other VMMs. As this problem only occurs for this specific VMM, it is probably not a general issue. The splitting of the value range into two subranges, one of them at very high values close to the maximum of 256, as seen in Figure 17c is observed for all of the VMMs. As it only occurs for a subset of runs, a comparison of the settings could yield a possible cause for the splitting.

4.8 Summary

Successful data acquisition, slow control and proof of principle for a variety of different settings of the VMM3 have been performed. The analysis of the test beam data revealed a number of problems and challenges with regards to some features of the VMM3. Some of the issues have already been addressed such as the correction for the SRS overflow or the trimming of the individual channel thresholds. The test beam in October is a promising opportunity to improve our understanding of the underlying issues as well as identifying and eliminating the cause.

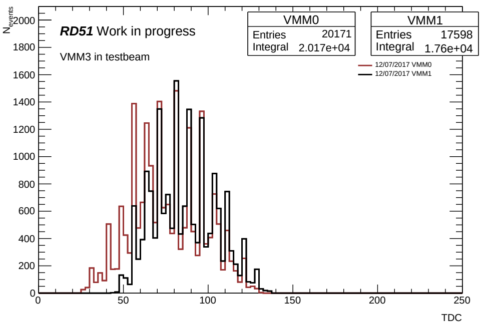

(a) TDC spectrum for Run 9.

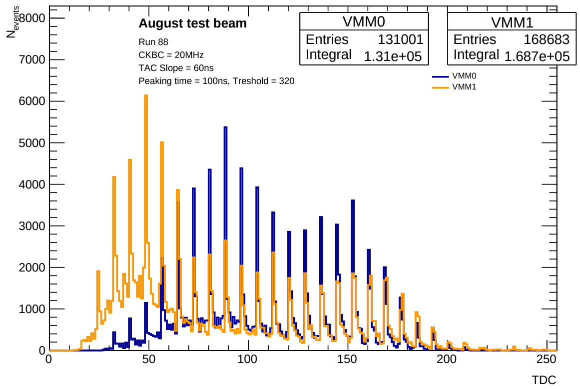

(b) TDC spectrum for Run 88.

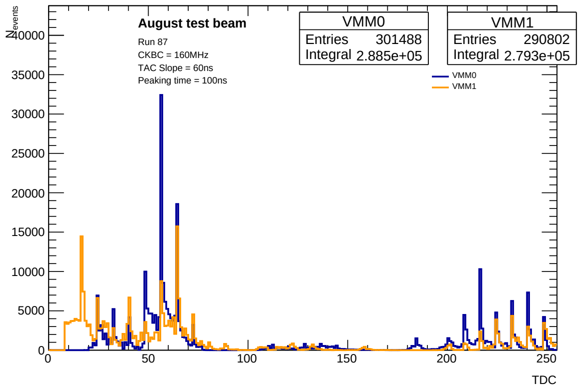

(c) TDC spectrum for Run 87.

Figure 17: TDC spectra for two VMMs showing different features that pose a starting point for further investigations.

References

[VMM] Polychronakos V., Iakovidis G., De Geronimo G.: *ATLAS NSW Electronics Specifications Component: VMM*, Version: v3.3 (2017)

[PFE] Pfeiffer D. et al.: *The μTPC method: improving the position resolution of neutron detectors based on MPGDs*, JINST (2015)